Time Reversal Terahertz Imaging

A. Boh Ruffin, *Member, IEEE*, J. Van Rudd, *Member, IEEE*, Joan Decker, Laurent Sanchez-Palencia, Lénaic Le Hors, John F. Whitaker, *Member, IEEE*, and Theodore B. Norris, *Associate Member, IEEE*

***Abstract*—We describe a technique for imaging in the terahertz regime using time reversal of single-cycle pulses. Specifically, the time-reversal symmetry of Maxwell's wave equation is exploited to reconstruct the transmission function of a diffracting aperture by inverting the diffracted fields. After deriving a time-reversed form of the Huygens–Fresnel diffraction integral, we demonstrate through simulation and experiment the reconstruction of one-dimensional and two-dimensional (2-D) objects. A means to obtain data efficiently for reconstruction of 2-D apertures is described. The spatial resolution determined by the Sparrow criterion is found to correspond to approximately 30% of the peak wavelength and 85% of the mean wavelength of the power spectrum of the single-cycle waveform. Finally, the modulation transfer function for the imaging method is simulated and is shown to be nearly diffraction-limited when compared to an ideal imaging system.**

***Index Terms*—Diffraction, inverse problem, terahertz imaging.**

I. Introduction

As THE technology for generating, measuring, and using single-cycle terahertz (THz) electromagnetic pulses has developed over the past two decades, the effects of diffraction on the spatiotemporal waveform have become an important subject. Spatiotemporal reshaping due to diffraction can be dramatic, since the spectrum of these pulses can span as much as three orders of magnitude. Several experimental and theoretical works have considered spatiotemporal reshaping in some detail [1]–[4]. The effects on the terahertz pulse profile due to Rayleigh and Mie scattering have been investigated by Cheville and co-workers [5], [6]. One of the interesting applications of terahertz single-cycle pulses is that they can be used as a laboratory for the investigation of effects of generic ultrabroad-band pulse propagation, whether the pulses are optical [7] or acoustic [8]. In this paper, we consider the diffraction of single-cycle pulses, and show that time reversal of the diffracted fields may be used as an inverse method of imaging and may also serve as a useful analogy for new imaging approaches using other forms of single-cycle pulses.

The inverse problem in physics often poses such questions as, "Can one hear the shape of a drum?" [9]. Inverse problems are found in a broad range of fields, for example, in imaging and object reconstruction in optics. The inverse method seeks to analyze scattered light to infer or reconstruct an object's shape. We present here a novel form of imaging using mathematically time-reversed broad-band scattered fields to reconstruct one- (1-D) and two-dimensional (2-D) objects. Typically, in inverse problems, one considers the diffraction or scattering of an incident narrow-band wave in the frequency domain; in this paper, however, we consider the scattering of extremely broad-band, single-cycle pulses to demonstrate a purely time-domain method for object reconstruction. Our technique is based on time-reversing scattered transients measured in the far-field and back-propagating these fields to the scattering object.

Direct problems in optics, of course, include diffraction, refraction, interference, absorption, spectroscopy, as well as imaging problems. The investigation presented here was in part inspired by developments in direct imaging schemes [10], [11]. Activities in terahertz-ray imaging have increased significantly since its first demonstration in 1995 by Hu and Nuss [12]. Notable developments include the terahertz Hall effect [13], tomographic terahertz imaging [14], single-shot imaging [15], and near-field terahertz-ray imaging [16], [17]. It is expected that terahertz imaging will continue to grow and find applications in industrial and medical settings [18]. Still, these techniques are classified as direct imaging methods. In addition to its potential utility for terahertz imaging in certain geometries, the inverse imaging technique we discuss in this paper may also serve as a model system for understanding time-reversal imaging in other systems (optical or acoustical) which employ single-cycle pulses. We also anticipate that our inverse terahertz imaging technique can be adapted to tomographic imaging techniques [19]–[22] to obtain three-dimensional (3-D) reconstructions.

In this paper, we expand and extend the discussion of the time-reversal imaging technique we first presented in [23]. We first revisit time-domain diffraction and then introduce the concept of time-reversal for object reconstruction in Section II. In Section III, we present experimental methods for the reconstruction of 1-D and 2-D objects using both transmissive and reflective geometries. Lastly, in Section IV, we discuss resolution limits and compare our technique to conventional (direct) terahertz-ray imaging.

II. Time-Domain Diffraction, Time Reversal, and Object Reconstruction

The diffraction theory of monochromatic light has been established in great detail [22]. The diffraction of nonmonochromatic light is also rather straightforward and can describe the

Manuscript received December 12, 2001; revised April 2, 2002. This work was supported in part by the National Science Foundation through the Center for Ultrafast Optical Science under Grant STC PHY 8920108, by the Air Force Office of Scientific Research, Air Force Material Command, USAF, under Grant F49620-98-1-0365, and by the Air Force SBIR Initiative under Contract F33615-98-C-2820. The work of A. B. Ruffin was supported by the National Physical Science Consortium and the University of Michigan Applied Physics Fellowships.

A. B. Ruffin, J. Decker, L. Sanchez-Palencia, L. Le Hors, J. F. Whitaker, and T. B. Norris are with the Center for Ultrafast Optical Science, The University of Michigan, Ann Arbor, MI 48109-1099 USA.

J. Van Rudd is with Picometrix, Inc., Ann Arbor, MI 48113-0243 USA.

Publisher Item Identifier 10.1109/JQE.2002.801007.

0018-9197/02$17.00 © 2002 IEEE

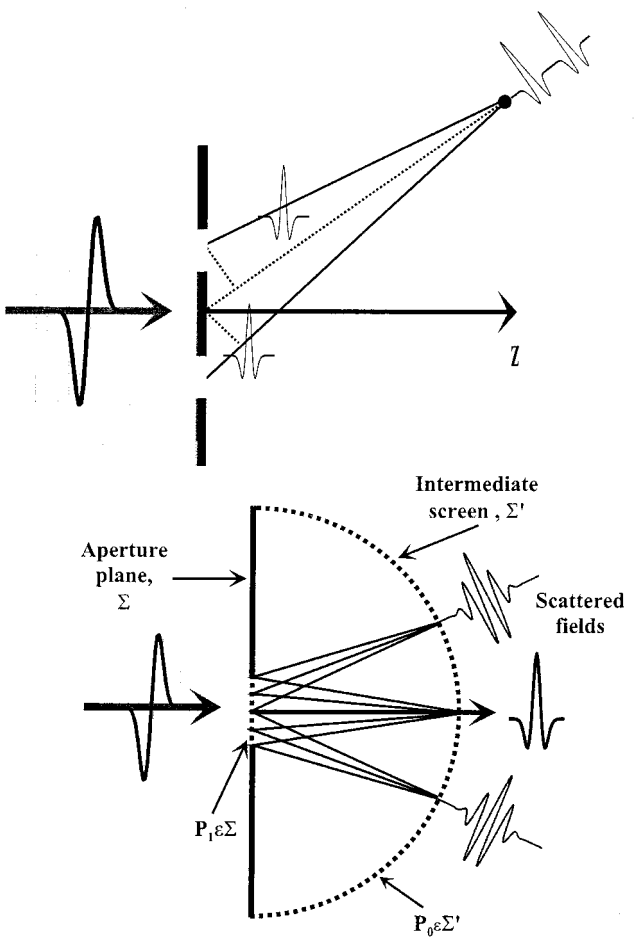

Fig. 1. Time-domain view of diffraction from (top) a double-slit and (bottom) a grating. In either case, impulses originating from adjacent points in the aperture plane will add coherently and give rise to the multicycle waveforms at the off-axis positions. Here, the lower figure defines the diffractive surfaces, the aperture plane, and intermediate screen in the far field.

spatiotemporal evolution of ultrawide broad-band electromagnetic pulses in both the frequency and time domains. For example, Nahata *et al.* [3] used a frequency-domain approach to account for the reshaping of terahertz pulses after diffracting through the narrow aperture of an electrooptic detector, whereas Bromage *et al.* and Budiarto *et al.* observed a similar temporal reshaping/transformation of terahertz pulses as the pulses propagated through conductive apertures and from the near-field of a large-aperture antenna. Coherent sampling techniques make it possible to retain both amplitude and phase information during the measurement of terahertz pulses, thus it is seemingly reasonable to cast transformations strictly in the time domain.

A time-domain view of diffraction is important for developing the idea of time reversal of diffracted waveforms. We begin by developing a pictorial view of diffraction. Consider the classical double slit problem in the time domain. The frequency-domain analysis of this example maintains that the phase differences between the two apertures lead to constructive or destructive interference at off-axis, far-field positions. However, these same phase differences correspond to temporal delays; thus, intuitively, each temporal feature of the scattered transient corresponds to the arrival of an impulse from a different region of the aperture, as illustrated in Fig. 1.

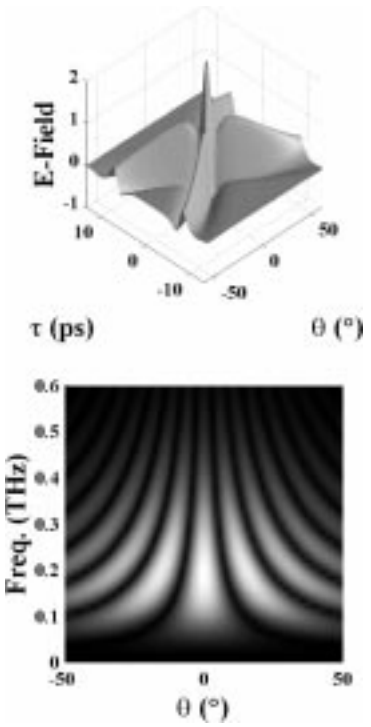

Fig. 2. (Top) Time-domain, far-field diffraction of an single-cycle pulse from a double slit. (Bottom) Corresponding frequency-domain spectra.

Now consider the diffraction of a single-cycle wavepacket from a double slit. The diffraction of broad-band electromagnetic pulses can be treated with the time-domain Huygens–Fresnel diffraction formula [22]

$$u(P_0, t) = \iint_{\Sigma} \frac{\cos(\hat{n}_0, \vec{r}_{01})}{2\pi c r_{01}} \frac{\partial}{\partial t} u\left(P_1, t - \frac{r_{01}}{c}\right) d\sigma \quad (1)$$

where $\cos(\hat{n}_0, \vec{r}_{01})$ is the zenith angle made with respect to the normal vector of the aperture, and the vector $\vec{r}_{01}$, where r_{01} is the distance from the object point P_1 to the far-field point P_0, and c is the speed of light. This integral can calculate the diffracted field, $u(P_0, t)$, from any input field, $u(P_1, t-(r_{01}/v))$, emanating from an area element $d\sigma$ in the aperture Σ. Equation (1) also provides insight to the on-axis, near- to far-field temporal transformation of the input pulse; namely, the far-field pulse is simply the time derivative of the input pulse. This transformation originates from the phase factor appearing in Huygens' integral [24]

$$U(P_0, \nu) = \frac{i}{\lambda} \iint_{\Sigma} U(P_1, \nu) \frac{\exp(ikr_{01})}{r_{01}} \cos(\hat{n}_0, \vec{r}_{01})\, d\sigma \quad (2)$$

that corresponds to the Gouy phase shift between the input field $U(P_1, \nu)$, and the far-field waveform $U(P_0, \nu)$. The time-derivative nature of this far-field transformation is also consistent with Feng's calculations where it was shown that the near- and far-field pulses are Hilbert transforms of one another [25], [26].

The result of propagating the single wavepacket through a double slit and recording the scattered fields at zenith and several positions along the spherical screen is shown in Fig. 2.

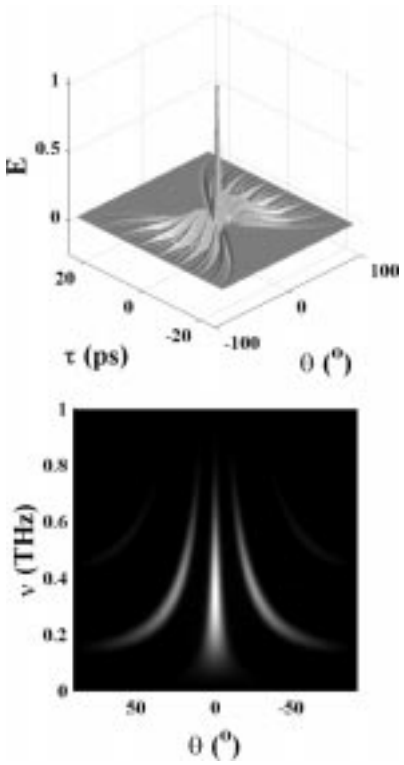

Fig. 3. (Top) Time-domain, far-field diffraction of a single-cycle Gaussian pulse from a seven-slit grating. (Bottom) Corresponding frequency-domain spectra calculated by Fourier transformation of the data in the top figure.

Here, we propagate a pulse with a beam waist and pulsewidth of 10 mm and 1.5 ps, respectively, to a distance of 30 cm for this simulation. The increased delay between the two pulses as the zenith angle increases from the on-axis position is clearly shown. This corresponds to an increase in the time of flight from the aperture to the observation position for the diffracted pulse as the zenith angle advances from $\theta = 0$ along the spherical screen. The corresponding power spectrum is illustrated in the lower half of Fig. 2; the structure in the spectrum is due to interference of different frequency components from the two slits.

This approach may be used to illustrate a time-domain view for the diffraction of a single-cycle, Gaussian wavepacket ($E(t) = t/\tau_p \exp[-2\ln 2(t/\tau_p)^2]$) through a grating. Fig. 1 illustrates how the waveforms at off-axis positions in the far-field result from contributions of impulses arriving at different time delays from the slits that comprise a grating. The far-field diffraction of the single-cycle wavepacket calculated from (1) is displayed in Fig. 3. The increase in the period of the diffracted transients with increasing angle is clearly apparent. From simple geometry, the time delay between pulses diffracted from two adjacent slits (which corresponds to the waveform period) is just $\Delta t = d\sin\theta/c$, where d is the distance between the two slits. By defining the wavelength as the spatial periodicity of the waveform, $\lambda = c\Delta t$, we find the usual grating equation (for first order diffraction) $\lambda = d\sin\theta$. Fig. 3 (lower) shows the angular dependence of the power spectrum calculated by Fourier transforming Fig. 3 (top), and as expected it conforms exactly to the grating equation.

Because of the time-reversal symmetry of Maxwell's equations and the corresponding solution of the wave equation, the

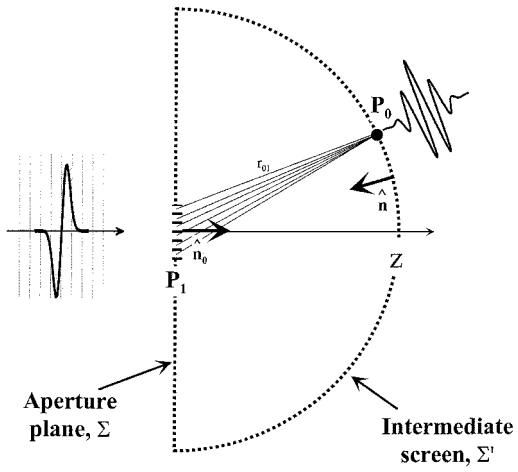

Fig. 4. Pictorial view of time reversal.

diffracted field at any far-field position can be mathematically time-reversed and then used as an input field in the time-domain Kirchhoff integral to reconstruct fields at a position P_1 on the the plane Σ, where $P_1 \in \Sigma$, as noted in Fig. 4. That is, it is possible to determine the (spatial) transmission function at Σ by using the terahertz waveforms measured at several off-axis positions P_0, and applying an algorithm for back-propagating and integrating these fields at positions P_1. The concept of time-reversibility and object reconstruction is pictorially represented in Fig. 4. We illustrate how the fields that emanate from the aperture Σ add in amplitude and phase (delay) at points on the intermediate screen. The *time-reversed* waveforms at the (spherical) intermediate screen, $u(P_1, t)$, can then back-propagate over the same paths as the forward going fields toward the aperture Σ. Thus, the spatial transmission function at the object plane will be given by the sum of the back-propagated fields (normalized to the input wave amplitude). In our simulations and experiments r_{01} is held constant, and is equivalent to observing or detecting the diffracted fields at a spherical screen. Keeping r_{01} constant greatly improved the speed of the numerical simulations as well as increasing the ease of maintaining a zero time origin during the experiments.

To derive a time-reversed equivalent of the Kirchhoff diffraction integral from the intermediate screen in Fig. 4, we begin with the frequency-domain diffraction formula [22] for a monochromatic field of frequency ν

$$U(P_1, \nu) = \frac{1}{4\pi} \iint_{\Sigma'} \left[U(P_0, \nu) \frac{\partial}{\partial n} \frac{\exp(ikr_{01})}{r_{01}} - \frac{\partial U(P_0, \nu)}{\partial n} \frac{\exp(ikr_{01})}{r_{01}} \right] d\sigma' \quad (3)$$

where $U(P_0, \nu)$ and $U(P_1, \nu)$ are scalar field amplitudes at the near- and far-field positions P_0 and P_1, respectively, and $\partial/\partial n$ is an inward normal derivative on the spherical surface in Fig. 4. The Kirchhoff and Rayleigh–Sommerfeld theories are typically used to derive simpler formulae for diffraction with the proper choice of Green's functions and boundary conditions. Equation (1) can readily be obtained through the Rayleigh–Sommerfeld formulation as shown in [22] and [27]. Because the Kirchhoff formulation is more general for curved diffracting surfaces, it

will serve to simplify the time-reversed formula for planar and nonplanar diffracting surfaces. Fourier transforming (3) to the time domain for back-propagation from the intermediate screen yields

$$u(P_1, t) = -\frac{1}{4\pi} \iint_{\Sigma'} \cdot \left\{ \frac{1}{cr_{01}} \cos(\hat{n}, \vec{r}_{01}) \left[\frac{\partial u}{\partial t} \right] + \frac{1}{r_{01}} \left[\frac{\partial u}{\partial n} \right] \right\} d\sigma' \quad (4)$$

where u is simply the time-domain form of U and the square brackets denote time-reversed fields evaluated at the position and time $(P_0, t + (r_{01}/c))$. As illustrated in Fig. 4, the field $u(P_0, t + (r_{01}/c))$ originated from the virtual source $(\partial/\partial t)u(P_1, t - (r_{01}/c))$ in the aperture plane, then through (4) the diffracted field $u(P_1, t)$ can be calculated from an input field $u(P_0, t+(r_{01}/c))$, from any surface, planar or nonplanar. In particular, (4) will determine the far-field disturbance emanating from the aperture Σ' (intermediate screen).

Consider the forward and backward propagation scheme shown in Fig. 4. To obtain a time-reversed diffraction integral for fields propagating backward from P_0 to P_1, substitute (1) into (4), but first observe that the normal derivative can be reexpressed as

$$\frac{\partial u}{\partial n} = \frac{\partial t}{\partial n} \frac{\partial u}{\partial t} \approx \frac{1}{c} \frac{\partial u}{\partial t} \quad (5)$$

since in the geometry of Fig. 4 $\partial t/\partial n$ is approximately $1/c$. From this, we ultimately obtain a time-reversed form of the Huygens–Fresnel diffraction integral.

$$U(P_1, t) = -\frac{1}{4\pi c} \iint_{\Sigma'} \left(\frac{\cos(\hat{n}, \vec{r}_{01}) + 1}{r_{01}} \right) \frac{\partial}{\partial t} u \cdot \left(P_0, t + \frac{r_{01}}{c} \right) d\sigma'. \quad (6)$$

This integral allows the spatial transmission function of the diffracting object to be reconstructed. It resembles the time-domain Rayleigh–Sommerfeld diffraction integral with the exception that the obliquity factor is now $(1 + \cos(n_0, \vec{r}_{01}))$. It is also interesting that our derivation for this integral is also consistent with the correction to Huygens' wave principle, as discussed by Miller [28]. He identified the failure of Huygens' original idea that wave propagation can be described in terms of simple effective sources on a wave front because no physical source can give rise to these wavelets. Miller, however, demonstrated that Huygens' principle is still valid, provided that the backward part of the wavelet, from a spatiotemporal dipole source, is considered

$$\phi(r_1, t) = -\int_{\Sigma} \left\{ \frac{(1 + \cos(\hat{n}, \vec{r}_{01}))}{4\pi r c} + \frac{\cos(\hat{n}, \vec{r}_{01})}{4\pi r^2} \right\} \cdot \frac{\partial}{\partial t} \phi \left(r_0, t - \frac{r}{c} \right) d\sigma \quad (7)$$

where ϕ is a scalar wave amplitude and the second term is neglected in the far field.

From (6), a straightforward back-propagation algorithm can be developed for the reconstruction of 1-D and 2-D diffracting objects. The algorithm first computes the time-reversed field $u_{mn}(P_{m0}, t_n + (r_{01}/c))$, numerically differentiates the diffracted waveform, and uses this as input into the integral in (6). In other words, at every position P_m on the far-field (intermediate screen, Σ'), and at every time, t_n, the field amplitude $u_{mn}(P_{m0}, t_n + (r_{01}/c))$ is back-propagated to all corresponding points of origins P_1 in the object plane Σ'. The back-propagation algorithm can be applied to simulated fields or fields from real data; the waveform corresponds to the electric field amplitude so the scattered transients contain all of the time delay (phase) information needed to reconstruct the spatial distribution of the electric field scattered from the object.

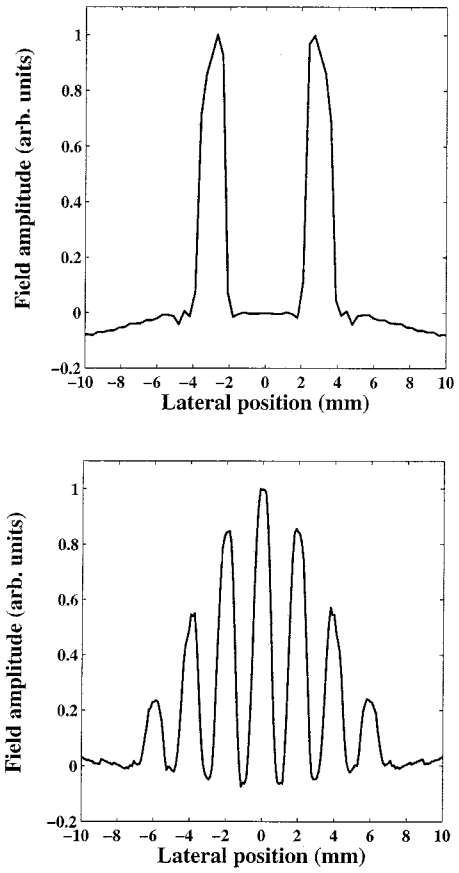

Fig. 5. 1-D object reconstructions for (top) the double-slit and (bottom) grating. The reconstructions were obtained using (6) with the simulation data in Figs. 2 and 3, respectively.

By applying our back-propagation algorithm with (6) to the simulation data in Figs. 2 and 3, we were able to reconstruct the transmission function of the double slit and grating, respectively. The reconstructions for the back-propagations are shown in Fig. 5. Clearly, the contrast for the 1-D objects is quite high. The simulations indicate the feasibility of the time-reversed imaging technique. In the next section, we discuss the experimental implementation of the idea.

III. Experiments

First we consider the reconstruction of a 1-D object, and then the reconstruction of 2-D objects. It should be noted that the algorithm that was used to reproduce the 1-D images in Fig. 5 can

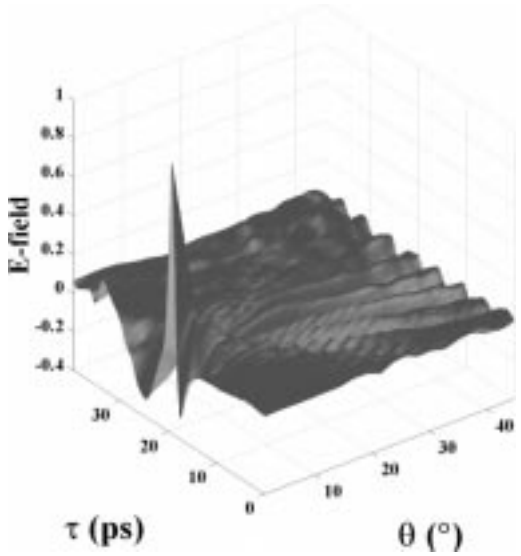

Fig. 6. Far-field scattered transients of an actual terahertz pulse on a (1-D) grating. Because of the symmetry of the object and high SNR, it was sufficient to measure on the half-plane $0^\circ \leq \theta \leq 40^\circ$ in Fig. 1.

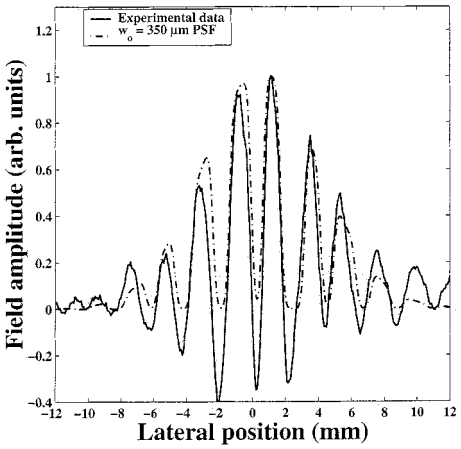

Fig. 7. 1-D object reconstruction for the grating used in the experiment (solid line). This reconstruction was obtained using (6) with the experimental data in Fig. 6. The experimental result is fit to a grayscale replica of the actual grating convolved with a 350-μm Gaussian point spread function (dotted line).

also be applied to 2-D objects. However, as the discussion develops, we will demonstrate a slightly modified means to reconstruct 2-D images that is more efficient and easier to implement in an actual terahertz system.

In the first set of experiments, we demonstrated the concept of time-reversal imaging using a 1-D object. A collimated terahertz beam with a diameter of approximately 3.0 cm was incident on a 14-slit, 1-mm feature size grating formed by Al foil strips on a low-density polyethylene substrate. The grating was oriented such that the incident terahertz pulse was crossed-polarized to the grating, and scattered the fields in a plane perpendicular to the grating axis (see the lower illustration in Fig. 1). The diffracted terahertz fields were measured at 62 zenith positions $(0^\circ \leq \theta \leq 45^\circ)$ at a radial distance of 25 cm centered on the object. This type of measurement required that the on-axis time-zero reference be maintained for all off-axis positions. This was accomplished by fixing the detector onto a rigid pivot arm and employing a commercially available, fiber-coupled terahertz measurement system (Picometrix, Inc., TR2000). Because the photoconductive transmitter and receiver were fiber-coupled, femtosecond optical pulses could be delivered to the photoconductive devices without the complications induced by a need to realign the optics and detector for each zenith position [29]. The system operates in the same manner as a conventional time-domain terahertz system [30] with the exception of the fiber coupling of the antennas and real-time data acquisition. Both emitter and receiver consisted of a 90° bow-tie antenna fabricated on low-temperature-grown GaAs (LT-GaAs) and were coupled to silicon aplanatic hyperhemispherical substrate lenses with a radius of 4 mm. The peak and mean frequencies, as well as the $1/e$ bandwidth of this photoconductive terahertz system were 175, 288, and 450 GHz, respectively. The receiving bow-tie antenna measured usable frequency components up to 700 GHz.

Fig. 6 shows the scattered terahertz fields measured at each zenith position on the intermediate screen. One can observe an increase in the scattered waveform's period for increasing angles as in the simulations of Figs. 2 and 3. The object was reconstructed by time-reversing the fields scattered from the grating (Fig. 6) and using these data as the input field $(\partial/\partial t)u(P_0, t + (r01/c))$ in (6). The image, shown in Fig. 7, is a plot of the electric field versus lateral position in the object plane, at a time delay corresponding to the peak of the pulse. The grating is successfully resolved, although the edge resolution is limited by the system bandwidth. From the edge response, determined by convolving the actual grating with a Gaussian point-spread function, we find the spatial resolution of the system to be approximately 350 μm (approximately a third of the peak wavelength).

We next demonstrated the principle of object reconstruction through the time reversal of scattered terahertz fields for 2-D objects. Ideally, in the 2-D case, the scattered fields should be measured at points on a spherical grid extending over the intermediate screen in both the zenith (θ) and azimuthal (ϕ) directions. Experimentally, however, it is difficult to move the photoconductive detector on a sphere centered at the object, since the pivot point would physically block or suppress the incident beam. This difficulty was circumvented by instead fixing the detector at a single angle, $\theta = \theta_d \neq 0$, and rotating the object about the z axis from 0 to 2π, as shown in Fig. 8. Rotation in ϕ of the object's frame of reference is entirely equivalent to the rotation of the detector on the sphere along the circle $\theta = \theta_d$, $0 \leq \phi \leq 2\pi$. This can be seen from two points of view.

Geometrically, since we are rotating the object through $0 \leq \phi \leq 2\pi$, it is sufficient to acquire data for only one zenith angle θ_d as all spatial frequencies in the object plane corresponding to $-\theta_d \leq \theta_{x,\,y} \leq \theta_d$ are accessed for both the x and y directions. From a time-domain perspective, we consider the transmission of the input plane wave after the object $u(P_1)$, to consist of a distribution of plane waves traveling in different directions away from the object. The field just after the aperture plane then is represented as

$$u(x_1, y_1, z = 0; t') = \int_{-\infty}^{+\infty} v(f_x, f_y; t') e^{i2\pi(f_x x + f_y y)}\, df_x\, df_y \quad (8)$$

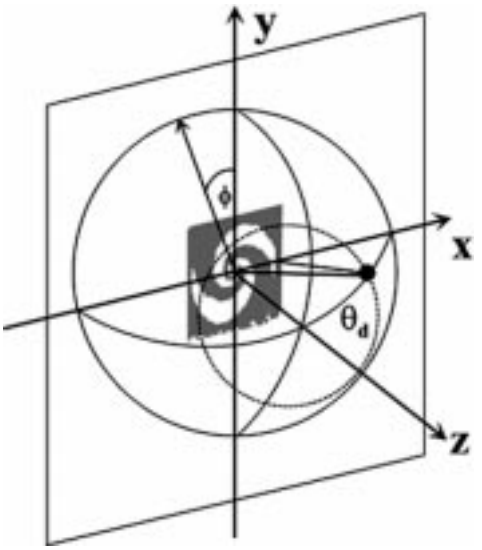

Fig. 8. 2-D experimental setup. Diffracted electric fields are measured at one off-axis position $\theta_d = 12^\circ$ as the object (spiral) was rotated about the z axis from 0 to 2π. The dashed circle represents equivalent measurement points at $\theta_d = 12^\circ$ on the spherical surface.

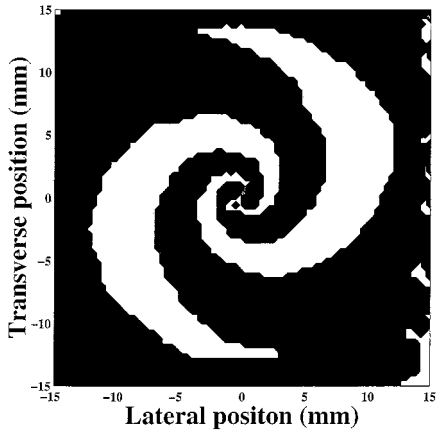

Fig. 9. Binary aperture used for the 2-D time-reversal imaging simulation. This figure depicts the 2-D object used in the experiment.

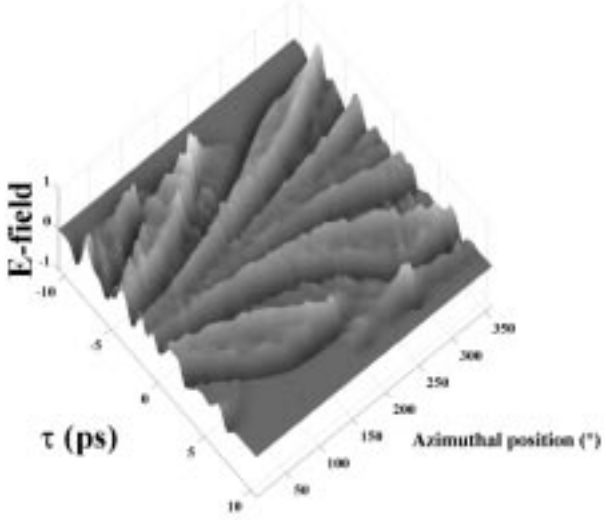

Fig. 10: Scattered fields at the intermediate screen for an electric field incident on the object in Fig. 9 for the 2-D time-reversal imaging simulation.

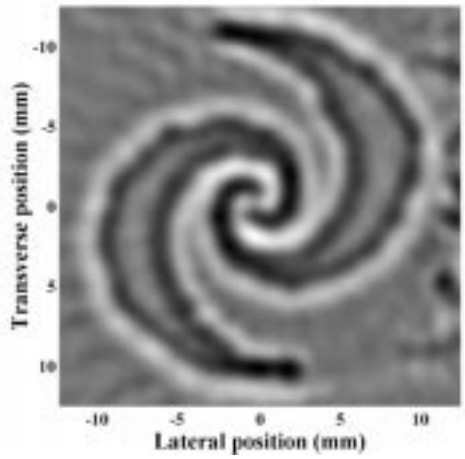

Fig. 11. Back-propagation result of the 2-D time-reversal imaging simulation calculated using (6) together with data in Fig. 10.

where t' is the retarded time in the forward direction, $v(f_x, f_y; t')$ is the spatial Fourier transform of the object's transmittance $u(x_1, y_1, z = 0; t')$, and $f_{x,y}$ are the spatial frequencies of the transmitted plane wave defined with respect to the direction cosines $f_{x,y} = \cos^{-1}(\alpha, \beta)/\lambda$. Because of the radial symmetry about the z axis for the diffraction scheme in Fig. 8, we only need to consider one transverse direction, say x, and the corresponding xz projection of the direction cosine, $\cos^{-1}(\alpha) = \theta_d$. Then for a broad-band input pulse which we consider to be a plane wave composed of many wavelengths, λ_i, we access the spatial frequencies

$$f_{x,y} = \frac{\theta_d}{\lambda_i} \tag{9}$$

that propagate to the far-field in the direction, θ_d. We therefore acquire spatial information (through phase delay information) about the object's transmission function as if we were measuring the diffraction of a monochromatic source at several positions.

To test the concept of 2-D time reversal imaging using the above scheme, we first performed a simulation by numerically propagating a single-cycle terahertz plane wave that best approximated the spatiotemporal profile of the actual beam onto a binary (amplitude) aperture identical to the one shown in Fig. 9. Using (6) the diffracted field was calculated with parameters identical to the experimental arrangement for the object oriented at $\phi = 0^\circ, 5^\circ, 10^\circ \cdots 360^\circ$ at a radial distance of 15 cm and at the zenith position $\theta_d = 12^\circ$. The calculated transient field at the intermediate screen is shown in Fig. 10. The time-reversal image was then calculated using (6) and is shown in Fig. 11. The object is clearly imaged and verifies the principle of ϕ-scanning for reconstruction of the object.

An experimental demonstration of the principle using these same parameters was implemented for a similar amplitude contrast object (an aluminum logarithmic spiral antenna pattern fabricated on fused silica) represented in Fig. 8. Acquiring data for only one zenith angle allowed the use of a conventional photoconductive free-space terahertz system. The system used here for the 2-D experiments had peak and mean frequencies of

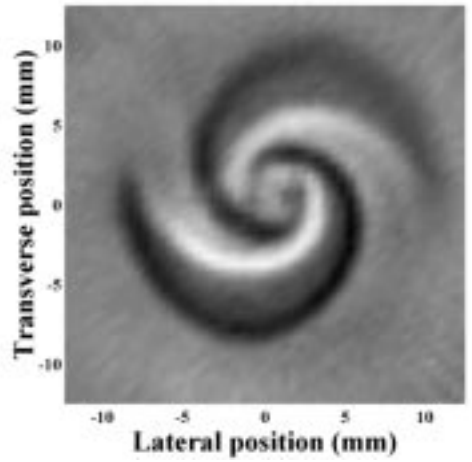

Fig. 12. Image obtained from the experimental data after performing the back-propagation algorithm described in the text.

136 and 377 GHz, with a $1/e$ bandwidth of 449 GHz and usable frequency components up to 1.3 THz. For the results presented here, the diffracted fields were measured at one zenith position ($\theta_d = 12°$) and 72 azimuthal positions (ϕ) between 0 and 2π. The result of the back-propagation and reconstruction is shown in Fig. 12 as a surface plot, wherein the opaque and clear portions of the aperture are clearly resolved, and in fact the system was able to resolve features smaller than the peak wavelength $\lambda_{\text{peak}} = 1.92$ mm. (It should be noted that no detector response deconvolution was used during the reconstruction of the image.) Ringing in the signal due to signal reflections in the photoconductive receiver is observed in the measured waveforms at the intermediate screen. This can contribute artifacts to the reconstructed image, but can be minimized by temporally "apodizing" the experimental waveforms. In fact, the image in Fig. 12 used the same data set to reconstruct the image in [23, Fig. 4], but was cropped to remove some of the artifacts in the background.

The ϕ-scanning technique can also image dielectric objects, i.e., objects which yield both amplitude and phase contrast. Following Goodman's approach to represent the Huygens–Fresnel integral in the time domain [27], when dispersion is negligible, it can be shown that the diffracted field from a dielectric object with transmission function $U(P_1, \omega) = T(P)\exp(-i\psi(P_1))$, where $\psi(P_1)$ is the time delay due to an object with a nonzero thickness, still yields the familiar time-dependent diffraction expression

$$u(P_0, t) = \int\int_{\Sigma} \frac{\cos(\hat{n_0}, \vec{r}_{01})}{2\pi c r_{01}} \frac{\partial}{\partial t} u(P_1, t - \psi)\, d\sigma \qquad (10)$$

where ψ represents the modified retarded time $((r_{01}/c) + \tau(P_1))$. Since (10) is congruent with the standard diffraction integral in (1), the identical back-propagation algorithm for such waveforms can also be used for the purpose of reconstructing a dielectric object's transmission function. Toward that end, the method for obtaining the image in Fig. 12 was repeated after replacing the amplitude object (spiral) with a dielectric object (plastic letter stencil). The resulting reconstruction is shown as a contour plot in Fig. 13. Here, the view was chosen to be slightly larger than the beam's diameter in order to demonstrate that the all features within the beam diameter can be imaged.

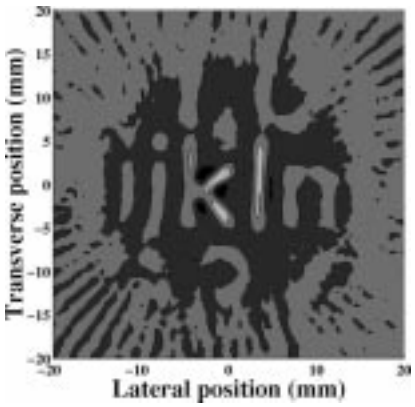

Fig. 13. 2-D reconstructed image of a phase contrast object (plastic letter stencil) measured in the transmissive geometry depicted in Fig. 8.

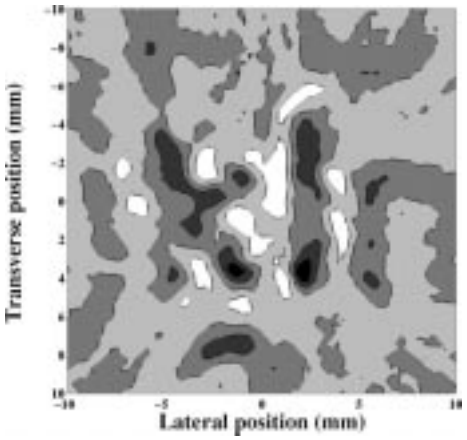

Fig. 14. Time-reversed image of the object in Fig. 13 obtained in a reflective configuration. The image quality suffers because the decreased SNR of reflected signals. Part of the "jklm" of Fig. 13 is imaged here.

Lastly we demonstrate a reflective geometry for which this technique might actually be applied in a radar (remote imaging) application. This scheme uses the same ϕ-scanning approach with the difference being that the transmitter and receiver are placed on the same side with respect to the 2-D object. The photoconductive antennas were first aligned such that the transmitted and reflected angles were equal to (45°) with respect to the normal of the object under test. Next the object was tilted 10° about the vertical axis (y axis, see Fig. 8) so that a diffracted order could be recorded between the rotation of the object in ϕ. The object used for this figure was the same letter stencil imaged in Fig. 13. The resulting imaging is depicted in Fig. 14; the reduced quality of the image is due to the lower SNR of the diffracted transients measured in the reflection mode.

IV. Resolution

Fig. 15 plainly reveals that the time-reversed ϕ-scanning technique (lower) produces images of quality comparable to direct (upper) imaging technique [11]. The greatest difference between the techniques would be the number of measurements required (i.e., the number of waveforms which must be acquired) to reproduce an object. For direct scanning, the step

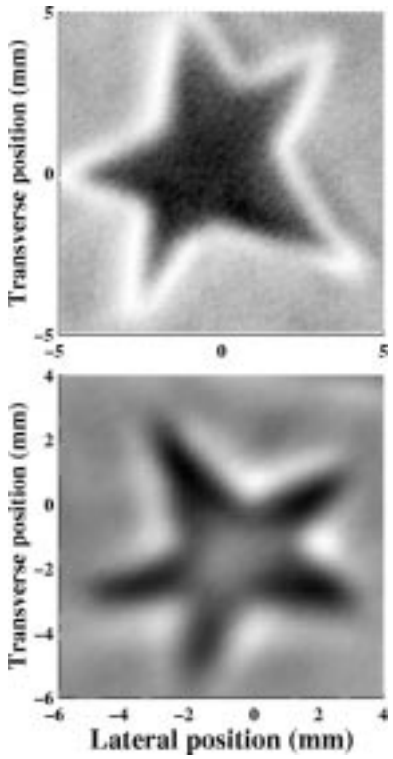

Fig. 15. Images of a 10 × 10 mm star pattern cut from a business card. (Top) Image obtained through conventional T-ray imaging. (Bottom) Image of the same star obtained through the time-reversed technique.

size of the lateral and transverse scanning gives the number of data points and, hence, the image quality. For example, the 1.1-mm pixel size in Fig. 15 (upper) required 8100 data points to produced a 90 × 90 image. Also, at each pixel, the time domain signal was Fourier transformed and integrated over the higher frequencies within the bandwidth (0.3–1.0 THz) to obtain maximum resolution. In contrast, the time-reversed method reproduced a 50 × 50 image with only 72 waveforms without any postprocessing of the data.

An estimation of the spatial resolution can be found through the 2-D time-domain imaging scheme by defining the resolution using a time-domain adaptation of the Sparrow criterion. Consider two temporal waveform measurements at the intermediate screen as one normally would two spatial point-spread functions in the context of imaging two point sources in the far-field. According to the Sparrow criterion [31], two pulses separated in time by Δt are resolved if there is a clear local minimum between the principal peaks of the two waveforms. If two object points separated by Δx give rise to waveforms separated by at least Δt at $\theta = \theta_d$, then they will be resolved. This temporal resolution limit Δt can then be translated into a lateral spatial resolution limit Δx in the object plane from simple geometric considerations

$$\Delta x = \frac{c\Delta t}{\sin\theta_d}. \tag{11}$$

In the 2-D experiment that produced the image in Fig. 12 through this criterion, the temporal resolution was 467 fs; thus we find that waveforms taken for orientations separated by $\Delta\phi = 15^\circ$ are resolved, as illustrated in Fig. 16. For

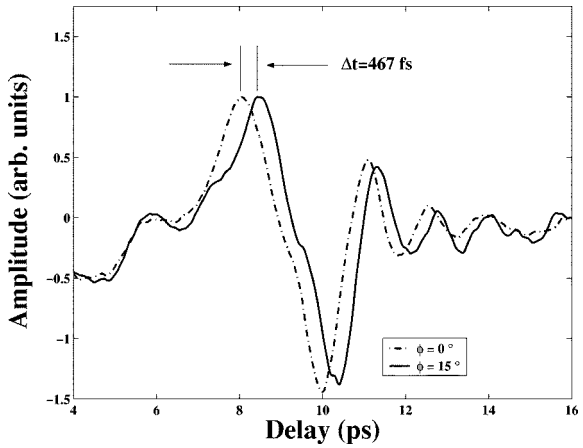

Fig. 16. Time-domain adaptation of the Sparrow criterion. Two electric field measurements at the intermediate screen for the $\phi = 0^\circ$ and $\phi = 15^\circ$ orientations. Applying a time-domain adaptation of the Sparrow criterion, we can say the two temporal peaks are resolved if there is a clear minimum between the two waveforms. From the delay between the waveforms and (11), the spatial resolution was determined to be 674 μm.

a detector position $\theta_d = 12^\circ$, this corresponds to a spatial resolution of $\Delta x = 674$ μm. Intuitively, one might expect the spatial resolution for imaging with single cycle pulses to be approximately equal to the wavelengths at which the power spectrum peaks or its centroid; for our system these are $\lambda_{\text{peak}} = 2.2$ mm and $\lambda_{\text{mean}} = 796$ μm, respectively. Thus, the actual spatial resolution obtained by the time-reversal imaging technique is approximately 30% of the peak wavelength and 85% of the mean wavelength of the single-cycle pulses used in this experiment. Improved spatial resolution can obviously be obtained by increasing the bandwidth of the terahertz system. The resolution can also be improved by measuring the terahertz waveforms at a larger θ_d. However, because the diffracted field strength drops off quickly at larger θ, the spatial resolution is limited in practice by the SNR of the system (for a fixed system bandwidth).

Another way of characterizing imaging systems is with the modulation transfer function (MTF). This can be simulated for this technique by measuring the contrast of 1-D gratings of different spatial frequencies. In conjunction with (1) and (6), we simulated such a measurement using a single-cycle pulse at a peak wavelength of 810 μm and a $1/e$ bandwidth of 602 GHz. A plot of the MTF against the grating dimension is shown in Fig. 17 (top). If we conservatively define an image exhibiting at least 50% contrast to be resolved, then we are able to image feature sizes approximately 2.3 times smaller than the peak wavelength at this bandwidth. It is also possible to compare the results of this experiment to the diffraction-limited imaging system [27], [32]. Plots of the diffraction-limited optical transfer function and the simulated MTF from the time-reversal technique are also shown in Fig. 17 (bottom). The spatial frequency axis of the MTF curve is normalized with respect to a cutoff frequency, defined to be the spatial frequency of the zero-contrast grating ($\rho_o = (2 \times 220\ \text{mm})^{-1}$). This graph plainly reveals that our technique could potentially produce near diffraction-limited images. In practice, however, we are limited by the SNR and the temporal resolution of the detector.

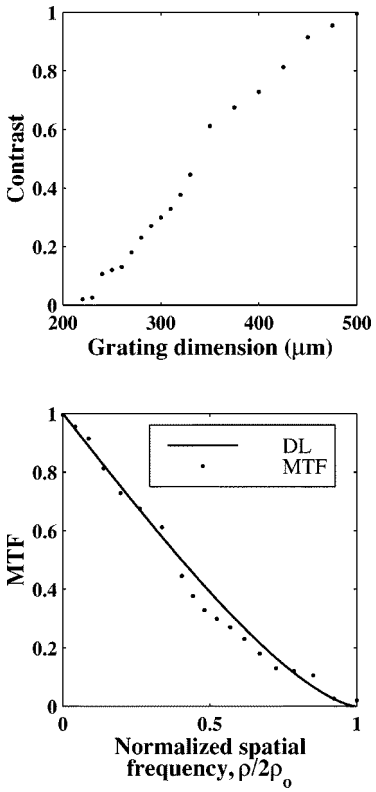

Fig. 17. (Top) Calculated contrast registered from images of gratings with various feature sizes. (Bottom) MTF for an ideal diffraction-limited and the time-reversed imaging systems.

V. Conclusion

By exploiting the time-reversal symmetry of the wave equation and the respective solution, we have derived a time-reversed equivalent of the time-domain Huygens–Fresnel diffraction integral. From this, we have devised a means to reconstruct 1-D and 2-D amplitude- and phase-contrast objects with the fields scattered from these objects. The images produced in both simulation and experiment have resolved features smaller than the peak and mean wavelength. Additionally, it was empirically illustrated that this technique might produce images rivaling that of an ideal diffraction-limited imaging system. Imaging via the time reversal of scattered fields is not exclusive to terahertz electromagnetic radiation. In fact, the technique will scale for other single-cycle pulses, including ultrashort optical or acoustic pulses.

Acknowledgment

The authors would like to acknowledge Dr. D. Zimdars for contributing the conventional T-ray image in Fig. 15.

References

[1] J. Bromage, S. Radic, G. Agrawal, C. R. Stroud, P. M. Fauchet, and R. Sobolewski, "Spatiotemporal shaping of half-cycle terahertz pulses by diffraction through conductive apertures of finite thickness," *J. Opt. Soc. Amer. B*, vol. 15, no. 4, p. 1399, 1998.

[2] E. Budiarto, N.-W. Pu, S. Jeong, and J. Bokor, "Near-field propagation of terahertz pulses from a large-aperture antenna," *Opt. Lett.*, vol. 23, no. 3, p. 213, 1998.

[3] A. Nahata and T. F. Heinz, "Reshaping of freely propagating terahertz pulses by diffraction," *IEEE J. Select. Topics Quantum Electron.*, vol. 2, p. 701, Sept. 1996.

[4] S. Feng and H. G. Winful, "Spatiotemporal transformation of isod-iffracting ultrashort pulses by nondispersive quadratic phase media," *J. Opt. Soc. Amer. A*, vol. 16, no. 10, p. 2500, 1999.

[5] R. A. Cheville and D. Grischkowsky, "Time domain terahertz impulse ranging studies," *Appl. Phys. Lett.*, vol. 67, no. 14, p. 1960, 1995.

[6] R. W. McGowan, R. A. Cheville, and D. Grischkowsky, "Time resolved measurements which isolate the mechanisms responsible for terahertz glory scattering from dielectric spheres," *Phys. Rev. Let.*, vol. 80, no. 2, pp. 269–273, Jan. 1998.

[7] A. Gurtler, C. Winnewisser, H. Helm, and P. U. Jepsen, "Terahertz pulse propagation in the near field and the far field," *J. Opt. Soc. Amer. A*, vol. 17, no. 1, pp. 74–83, 2000.

[8] J. V. Rudd, R. G. Baraniuk, W. W. Symes, T. D. Dorney, J. L. Johnson, and D. M. Mittlelman, "Terahertz reflection imaging using kirchhoff migration," *Opt. Lett.*, vol. 26, no. 19, pp. 1513–1515, Oct. 2001.

[9] M. Kac, "Can one hear shape of a drum," *Amer. Math. Monthly*, vol. 73, no. 4P2.

[10] D. M. Mittleman, R. H. Jacobsen, and M. C. Nuss, "T-ray imaging," *IEEE J. Select. Topics Quantum Electron.*, vol. 2, no. 3, pp. 967–692, Sept. 1996.

[11] D. M. Mittleman, M. Gupta, R. Neelamani, R. G. Baraniuk, J. V. Rudd, and M. Koch, "Recent advances in terahertz imaging," *Appl. Phys. B*, vol. 68, pp. 1085–1094, 1999.

[12] B. B. Hu and M. C. Nuss, "Imaging with terahertz waves," *Opt. Lett.*, vol. 20, no. 16, pp. 1716–1720, Aug. 1995.

[13] D. M. Mittleman, J. Cunningham, and M. C. Nuss, "Noncontact semiconductor wafer characterization with the terahertz hall effect," *Appl. Phys. Lett.*, vol. 71, no. 1, pp. 16–18, July 1997.

[14] D. M. Mittleman, S. Hunsche, L. Boivin, and M. C. Nuss, "T-ray tomography," *Opt. Lett*, vol. 22, no. 12, pp. 904–906, 1997.

[15] Z. Jiang and X.-C. Zhang, "Single-shot spatiotemporal terahertz field imaging," *Opt. Lett.*, vol. 23, no. 14, pp. 1114–1116, July 1998.

[16] S. Hunsche, M. Koch, I. Brener, and M. C. Nuss, "THz near-field imaging," *Opt. Commun.*, vol. 150, pp. 22–26, May 1998.

[17] Q. Chen, Z. Jiang, G. X. Xu, and X.-C. Zhang, "Near-field terahertz imaging with a dynamic aperture," *Opt. Lett.*, vol. 25, no. 15, pp. 1122–1124, Aug. 2000.

[18] G. C. Cho, P. Y. Han, and X.-C. Zhang, "Time-domain transillumination of biological tissues with terahertz pulses," *Opt. Lett.*, vol. 25, no. 4, pp. 242–244, February 2000.

[19] A. C. Kak and M. Slaney, *Computerized Tomographic Imaging*, 1st ed. New York: IEEE Press, 1988.

[20] T. D. Dorney, J. L. Johnson, and D. M. Mittleman, "Enhanced depth resolution in terahertz imaging using phase-shift interferometry," *Appl. Phys. Lett.*, vol. 78, no. 6, pp. 835–837, Feb. 2001.

[21] T. D. Mast, "Wideband quantitative ultrasonic imaging by time-domain diffraction tomography," *J. Acoust. Soc. Amer.*, vol. 106, no. 6, pp. 3061–3071, Dec. 1999.

[22] M. Born and E. Wolf, *Principles of Optics*, 7th ed. Cambridge, U.K.: Cambridge Univ. Press, 1997.

[23] A. B. Ruffin, J. Decker, L. Sanchez-Palencia, L. Lehors, J. F. Whitaker, T. B. Norris, and J. V. Rudd, "Time reversal and object reconstruction using single-cycle terahertz pulses," *Opt. Lett.*, vol. 26, no. 10, pp. 681–683, May 2001.

[24] A. E. Siegman, *Lasers*. Sausalito, CA: University Science Books, 1986. Note that Gouy's name is misspelled as "Guoy" in this reference.

[25] H. G. Winful, S. Feng, and R. W. Hellwarth, "Spatiotemporal evolution of focused single-cycle electromagnetic pulses," *Phys. Rev. E*, vol. 59, no. 4, pp. 4630–4649, 1999.

[26] S. Feng and H. G. Winful, "Physical origin of the Gouy phase shift," *Opt. Lett.*, vol. 26, no. 8, pp. 485–487, 2001.

[27] J. W. Goodman, *Introduction to Fourier Optics*, 2nd ed. New York: McGraw-Hill, 1996.

[28] D. A. B. Miller, "Huygens's wave propapagation principle corrected," *Opt. Lett.*, vol. 16, no. 18, pp. 1370–1372, 1991.

[29] J. V. Rudd, D. Zimdars, and M. Warmuth, "Compact, fiber-pigtailed, terahertz imaging system," in *Photonics West: Conf. on Commercial and Biomedical Applications of Ultrafast Lasers II* San Jose, CA, 2000, vol. II.

[30] M. van Exter, C. Fattinger, and D. Grischkowsky, "High-brightness terahertz beams characterized with an ultrafast detector," *Appl. Phys. Lett.*, vol. 55, no. 4, p. 337, 1989.

[31] D. Guenther, *Modern Optics*, 2nd ed. New York: John Wiley and Sons, 1990.

[32] C. S. Williams and O. A. Becklund, *Introduction to the Optical Transfer Function*. New York: Wiley, 1989.

A. Boh Ruffin (M'01) was born in Flint, MI, in 1972. He received the A.B. degree in physics from the University of Michigan-Flint in 1995 and the M.S. and Ph.D. degrees in applied physics from the University of Michigan, Ann Arbor, in 1999 and 2001, respectively.

While a graduate student he held the University of Michigan Applied Physics Fellowship and the National Physical Science Consortium Fellowship. His graduate research was on diffraction-induced effects on single-cycle terahertz pulses. He currently is a Senior Research Scientist for Corning, Inc.

Dr. Ruffin is a member of the National Society of Black Physicists, the IEEE Lasers and Electro-Optics Society, and the Optical Society of America.

J. Van Rudd (M'01) was born in Seattle, WA, in 1965. He received the B.S. degree in physics from the University of California at Davis in 1988 and the M.S. and Ph.D. degrees in electrical engineering from the University of Michigan, Ann Arbor, in 1991 and 1994, respectively.

He joined Picometrix, Inc., Ann Arbor, MI, in 1994, and ran the Ultrafast Instrumentation group from its inception in 1994 through December 2000, where he developed the world's first commercially available time-domain terahertz system. Since December 2000, he has been the Director of Engineering at Picometrix.

Dr. Rudd is a member of the Optical Society of America and the IEEE Lasers and Electro-Optics Society.

Joan Decker, photograph and biography not available at the time of publication.

Laurent Sanchez-Palencia was born in Paris, France, in 1975. He is currently working toward the Ph.D. degree at the Laboratoire Kastler-Brossel at the Ecole Normale Supérieure in Paris, France, under Prof. G. Grynberg.

While an undergraduate student at the Ecole Polytechnique, Palaiseau, France, he earned a visiting research fellowship to the Center for Ultrafast Optical Science at the University of Michigan, Ann Arbor, in 1999 to study under Prof. T. Norris. His current research interests include nonlinear optics and the dynamics of laser cooled atomic samples in optical lattices.

Lénaic Le Hors was born in La Rochelle, France, in 1975. He received degrees from the Ecole Polytechnique, Palaiseau, France, and the Ecole Supérieure Optique, Orsay, France.

While an undergraduate, he earned a Visiting Research fellowship to the Center for Ultrafast Optical Science, University of Michigan at Ann Arbor, in 1998 to study under Prof. T. Norris. After two years of research on active polarimetric imaging at the Thales Laboratoire Central de Recherche, Orsay, France, he joined the European space company Astrium, Toulouse, France, in 2001. He is now involved in advanced studies on space lidars and other optical instruments.

John F. Whitaker (S'84–M'88) received the B.Sc. degree in physics from Bucknell University, Lewisburg, PA, and the M.Sc. and Ph.D. degrees in electrical engineering from the University of Rochester, Rochester, NY.

He joined the faculty of the Department of Electrical Engineering and Computer Science at the University of Michigan, Ann Arbor, in 1989. He currently holds the titles of Research Scientist and Adjunct Professor, and he is the Coordinator of the Ultrafast Technology Area in the NSF Center for Ultrafast Optical Science. In 1995, he was also appointed to the position of Visiting Professor, First Class, at the University of Savoie in France. His research interests involve ultrafast-response optoelectronic materials, devices, and test and characterization techniques, as well as guided and free-space-radiating, terahertz-bandwidth pulses and their applications.

Dr. Whitaker is a member of the IEEE Microwave Theory and Techniques and Lasers and Electro-Optics Societies, and he was a recipient of the 1996 Microwave Prize from the IEEE Microwave Theory and Techniques Society.

Theodore B. Norris (A'95) received the B.A. degree in physics (with highest honors) from Oberlin College, Oberlin, OH, in 1982, and the Ph.D. degree in physics from the University of Rochester, Rochester, NY, in 1989, with a dissertation on time-resolved tunneling in semiconductor heterostructures.

He is a Professor in the Electrical Engineering and Computer Science (EECS) Department, University of Michigan, Ann Arbor. During 1989–1990, he continued his investigations of time-resolved optical studies of semiconductors at Thomson-CSF, France. He was an Assistant Research Scientist at the Ultrafast Science Laboratory (1990–1992), an Assistant Professor (1992–1996), and an Associate Professor in EECS (1996–2001), at the University of Michigan. His research interests include the application of femtosecond optical techniques to the physics of semiconductor structures, the development of new ultrafast optical and electronic probes with high spatial resolution for applications to semiconductor nanostructures and biological imaging, and developing new laser sources for applications in femtosecond spectroscopy and the generation of terahertz radiation. This work has appeared in over 85 journal and 130 conference publications. His research is performed at the National Science Foundation Center for Ultrafast Optical Science and the Electrical Engineering and Computer Science Department at the University of Michigan.

Dr. Norris is a Fellow of the Optical Society of America and a member of the American Physical Society and the IEEE Lasers and Electro-Optics Society.